Biotemplated Hierarchical Nanostructure of Layered Double Hydroxides with Improved Photocatalysis Performance

Yufei Zhao,[†] Min Wei,[†,*] Jun Lu,[†] Zhong Lin Wang,[‡,*] and Xue Duan[†]

[†]State Key Laboratory of Chemical Resource Engineering, Beijing University of Chemical Technology, Beijing 100029, People's Republic of China, and [‡]Center for Nanoscience and Nanotechnology, School of Materials Science and Engineering, Georgia Institute of Technology, Atlanta, Georgia 30332-0245

ABSTRACT We report a biomorphic hierarchical mixed metal oxide (MMO) framework through a biotemplated synthesis method. A uniform Al_2O_3 coating was deposited on the surface of the biotemplate with an atomic layer deposition (ALD) process, and the film of ZnAl-layered double hydroxide (ZnAl-LDH), which faithfully inherits the surface structure of the biotemplate, was prepared by an *in situ* growth technique. Subsequently, a polycrystal ZnAl—MMO framework obtained by calcination of the LDH precursor has been demonstrated as an effective and recyclable photocatalyst for the decomposition of dyes in water, owing to its rather high specific surface area and hierarchical distribution of pore size. Therefore, the new strategy reported in this work can be used to fabricate a variety of biomorphic LDHs as well as MMO frameworks through replication of complicated and hierarchical biological structures for the purpose of catalysis, adsorbents, and other potential applications.

KEYWORDS: atomic layer deposition · biotemplated synthesis · hierarchical structure · LDH · photocatalysis

Hierarchical porous materials (micro-/meso-/macroporous) have attracted significant attention owing to their important role played in the diffusion of guest species through an inorganic network of pores and channels and their technological promise in many applications, including catalysis, sorption, and separation.[1,2] The combination of multiscaled porosity integrated into one moldable structure has been demonstrated to be an effective solution for yielding improved overall performances of the materials.[3] To create such structures, man-made templates such as bubbles, colloids,[4] polymers,[5,6] surfactant,[7] and porous anodic alumina[8,9] have been widely used. However, they generally lack inherent complexity and hierarchical architecture, making it impossible to synthesize materials with unique multiscale structures and morphologies.[10]

Nature provides many examples of biological materials with complicated, optimized, and efficient hierarchical morphologies and a large variety of porous structures from nanometer to macroscopic scale, which have been found to exhibit superior performance and efficiency in chemical and physical processes.[11,12] Among the prevalent approaches to achieve these advanced biological materials, learning from how structural materials can assemble themselves, now known as biomimetic materials chemistry, is perhaps the most promising method toward future innovations in discovering new structures and improving corresponding performances.[13]

Owing to the inexpensive, abundant, environmentally benign, and renewable biological resources provided by nature, scientists have long been interested in understanding the basic principles of the biological organizations assembled by highly order functional units and preparing inorganic materials by biological templates. For instance, researchers can fabricate such biostructures with high reproducibility and low-cost by utilizing biotemplate and coating it uniformly up to atomic thickness with an inorganic material. Mann and co-workers have successfully used bacteria, pollen grain, and some other organisms as templates to morphosynthesize silica, calcium carbonate, and calcium phosphate.[14,15] Sandhage *et al.* employed diatoms to synthesize silicon nanocrystals with intricate and well-controlled 3D morphologies at low temperature.[16] Later, the same group reported continuous nanocrystalline rutile TiO_2-based coating on 3D nanostructured butterfly templates by the sol−gel technique.[17] Up to now, several kinds of biological templates, such as pollen grain,[15] butterfly wing,[18] shells,[19] living cells,[20] rod-like

*Address correspondence to weimin@mail.buct.edu.cn, zhong.wang@mse.gatech.edu.

Received for review August 21, 2009 and accepted November 17, 2009.

Published online November 23, 2009.
10.1021/nn901055d

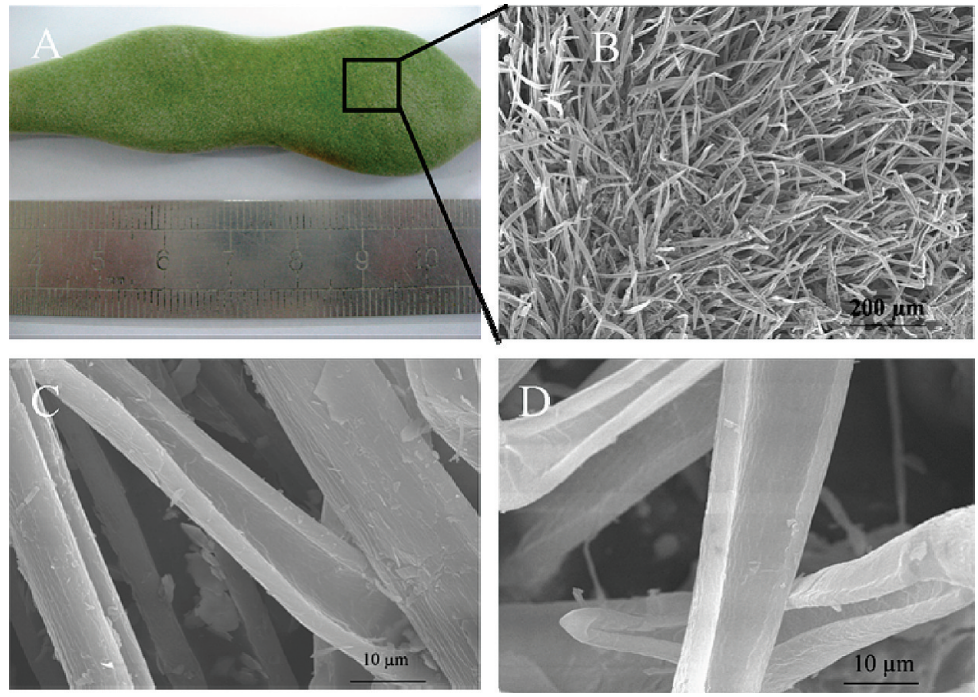

Figure 1. (A) Optical photograph of the legume; SEM images of the tubular trichome on the surface of the legume at (B) a low magnification and (C) a high magnification; (D) SEM image of the trichome with 600 deposition cycles of Al_2O_3 (~60 nm in thickness).

bacteria and viruses,[21] peptide,[22] and DNA,[23] have been utilized to synthesize inorganic materials for the development of catalysis,[24] separation, gas sensing,[16] optical,[18] electronic,[25] lithium secondary battery,[20] and biomedical applications.[26]

Layered double hydroxides (LDHs) are layered anionic clays generally expressed by the formula $[M^{II}_{1-x}M^{III}_x(OH)_2](A^{n-})_{x/n} \cdot mH_2O$ (M^{II} divalent and M^{III} trivalent metals, respectively, A^{n-} n valent anion).[27] Calcination of LDHs at intermediate temperature (300−600 °C) leads to the formation of mixed metal oxides (MMOs), which exhibit porous structure and high thermal stability.[28] On the basis of their versatility in chemical composition and high dispersion of metal oxides, LDH and MMO materials have been widely used as catalysts and supports, adsorbents for environmental remediation, and carriers for biological materials. Recently, the preparation of LDH and MMO films is a fast-growing research field for effective manipulation and application compared with the powder form.[29] Some researchers reported the LDH films by using hydrolysis of alkoxide-intercalated LDH derivatives, ultrasonification, and layer-by-layer technique.[30−32] Our group has recently reported the preparation of the LDH films by means of an *in situ* hydrothermal preparation on porous anodic alumina/aluminum substrate; moreover, both the superhydrophobic properties and corrosion-resistance for the underlying aluminum were investigated in detail.[33,34] Besides LDH films with 2D structure, Leroux *et al.* reported well-organized 3D macroporous LDHs by employing a colloidal crystal polymer as template.[35] Although there have been some morphology and architecture studies on LDH materials, to the best of our knowledge, biological organisms have not been previously utilized for the formation of LDH materials. By virtue of the advantages of biotemplates, it is feasible to obtain functional LDH materials with complicated and hierarchical morphologies for potential applications.

We report herein a general and facile method to fabricate ZnAl−LDH film and the resulting calcination product (MMO framework) through a biotemplated synthesis technique and demonstrate its effective and recyclable photocatalysis for the decomposition of two kinds of dyes in water, that is, sulforhodamine B (RB) and a azobenzene-containing polymer poly{1-4[4-(3-carboxy-4-hydroxyphenylazo)benzenesulfonamido]-1,2-ethanediyl sodium salt} (PAZO). A kind of legume was chosen as the biotemplate in this work, with specific tubular trichome on the surface (Figure 1). It was found that the biotemplated ZnAl−MMO framework exhibits 2.4 times higher BET specific surface area and much wider pore size distribution than the comparison sample (ZnAl−MMO powder), accounting for its enhanced photocatalytic performances. Therefore, this work not only provides a new biomimetic synthesis of hierarchical nanocrystalline LDH films and resulting MMOs framework but also gives demonstration of the prospective application in the field of photocatalysis.

Our strategy includes three steps, as shown in Scheme 1. First, a uniform Al_2O_3 coating on the surface of the legume was fabricated through a low-temperature atomic layer deposition (ALD) process. This process preserves the shape and fine structures of

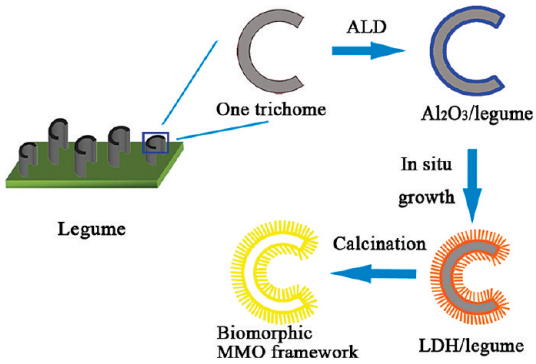

Scheme 1. Schematic representation for the fabrication of biotemplated LDH film and MMO framework from the legume. One trichome on the surface of the legume is chosen to illustrate the fabrication procedure.

the template but replaces the organic material by inorganic materials. Second, the ZnAl−LDH film, which faithfully inherits the initial surface structure of the legume, was prepared by an *in situ* growth technique. Finally, the polycrystal ZnAl−MMO framework was obtained by sacrificial template method through calcination of the LDH film precursor.

RESULTS AND DISCUSSION

Morphology and Structure of Biotemplated LDH and MMO. The legume chosen in this work is the fruit of a kind of wistaria. Numerous unclosed tubal trichomas can be observed on the exterior surface of the legume, with the diameter of ~10 μm (shown in Figure 1A−C). Atomic layer deposition (ALD) technique, which has emerged as a fast-growing subfield of nanotechnology research for the fabrication of controllable morphologies with high uniformity and precisely controlled thickness,[18,36] was used to replicate the biostructure of the legume by 600 cycles of Al_2O_3 film (~60 nm), as shown in Figure 1D. Comparison between panels C and D of Figure 1 shows that no obvious change in surface morphology can be observed after coating with Al_2O_3. By an *in situ* growth procedure reported by our group previously,[33] ZnAl−LDH film came into formation based on the Al_2O_3 coating deposited on the surface of legume. Figure 2A exhibits the surface view of the biotemplated LDH film, which faithfully inherits the initial surface structure of the legume, and high magnification (Figure 2B) shows curved and porous LDH crystal films on the surface of the trichoma. After calcination at 500 °C for 6 h, the as-grown curved crystals completely transferred to sheet-like nanocrystals perpendicular to the substrate (Figure 3A,B), affording multilevel structures including an array of ordered mesopores as well as macropores (Figure 3B,C). However, the comparative powder sample of ZnAl−MMO exhibits randomly oriented particles with aggregation and irregular morphology (see Supporting Information Figure S1). The XRD pattern (see Supporting Information Figure S2) of the biomorphic MMO framework displays the coexistence of reflections attributed to a ZnO phase (JCPDS file No. 36-1451)[37] as well as a $ZnAl_2O_4$ phase (JCPDS file No. 05-0669),[28] which is in accordance with the XRD pattern of the comparison sample (the ZnAl−MMO powder, see Supporting Information Figure S3). The energy-dispersive X-ray spectrometry (EDX) analysis of the ZnAl−MMO framework (Figure 3D) shows the presence of Zn, Al, O, and C, with a Zn/Al molar ratio of ~2.0. The results above indicate that the as-grown biotemplated LDH/legume transformed into a $ZnO/ZnAl_2O_4$ MMO framework which mimics the original macroarchitecture of the legume. The calcination process results in both the phase transformation and the decomposition of the biotemplate.

To further investigate the structural information of the ZnAl−LDH/legume and its calcination product, the materials were detected by high-resolution transmission electron microscopy (HRTEM). Figure 4A reveals that the ZnAl−LDH film on the legume is crystalline, as evidenced by well-defined lattice fringes in some regions. The hexagonal lattice with $a = 0.30$ nm corresponding to the (100) plane of the ZnAl−LDH phase was observed in the HRTEM image. Figure 4B shows the electron diffraction pattern of the nanocrystallite for the same sample, and the diffraction rings can be indexed as from the ZnAl−LDH phase.[38] The calcination product of the ZnAl−LDH/legume was also investigated by HRTEM, as shown in Figure 4C,D. Figure 4C displays the hexagonal nanocrystal of the ZnAl−MMO framework with a particle size of ~1 μm, which approximately agrees with the SEM image (Figure 3B). Figure 4D exhibits a typical HRTEM image at higher mag-

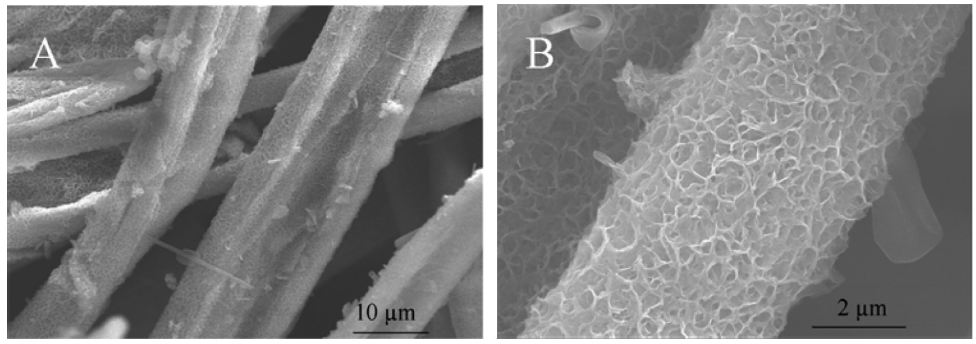

Figure 2. SEM images of the *in situ* growth LDH/legume film at low magnification (A) and high magnification (B).

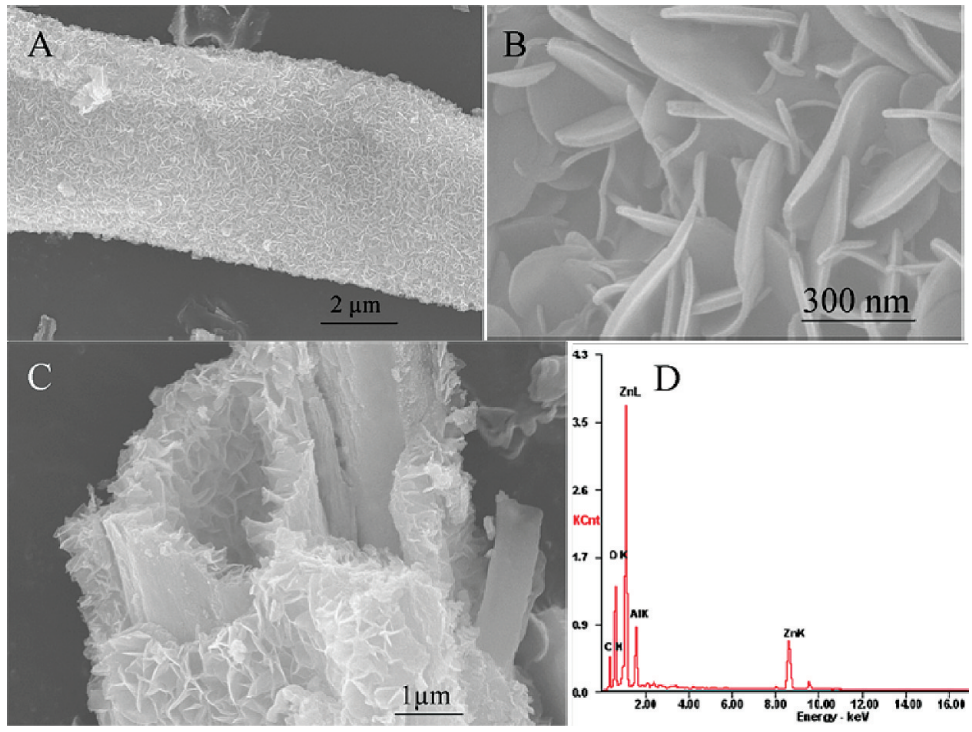

Figure 3. SEM images of the ZnAl−MMO framework obtained by calcination of LDH/legume precursor for the surface view at low (A) and high magnification (B); (C) section view and (D) corresponding EDX spectrum of the biomorphic ZnAl−MMO framework revealing the presence of Zn, Al, O, and C.

nification of the ZnAl−MMO framework. Interplanar distances of 0.24 and 0.28 nm can be determined for two separate nanocrystals, corresponding to the (311) plane of cubic $ZnAl_2O_4$ and the (100) facet of hexagonal ZnO,[28,37] which is consistent with the electron diffraction pattern (Figure 4E). Figure 4F shows the hexagonal nanocrystal ZnO with the interplanar distance of 0.28 nm, in accordance with the hexagonal wurtzite structure with the space group C_{6v}.[39] The results above unambiguously confirm that the wurtzite crystalline ZnO and cubic $ZnAl_2O_4$ structure formed through calcination process of the biotemplated LDH film. For comparison, HRTEM images for the ZnAl−LDH and ZnAl−MMO powder samples were obtained (Support-

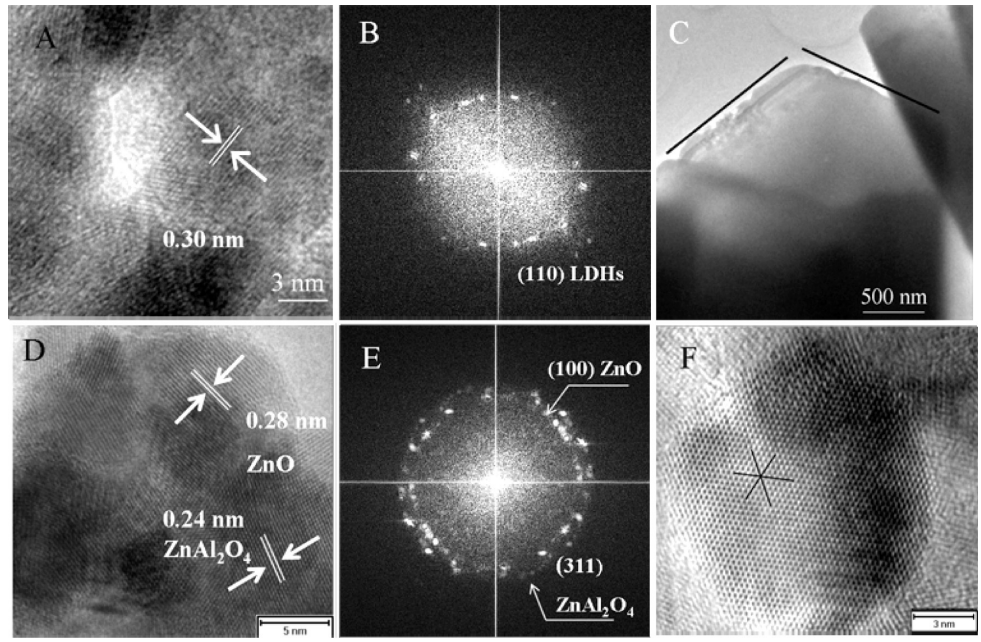

Figure 4. (A) HRTEM image of the ZnAl−LDH/legume; (B) electron diffraction pattern of the ZnAl−LDH/legume; HRTEM images of the ZnAl−MMO framework obtained from the ZnAl−LDH/legume at (C) low magnification and (D) high magnification; (E) electron diffraction pattern of the ZnAl−MMO framework; (F) HRTEM image of the ZnO nanocrystal.

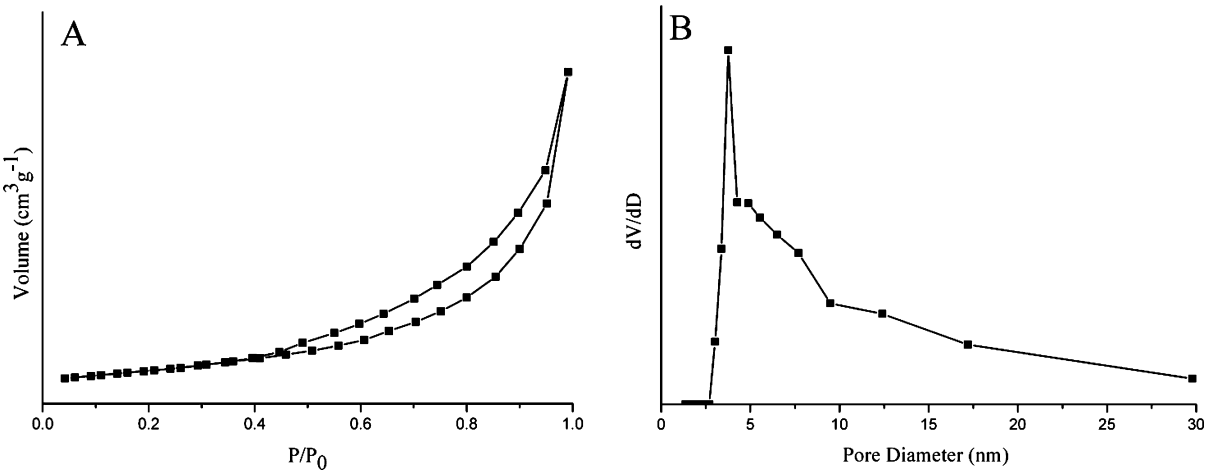

Figure 5. (A) N_2 sorption isotherm and (B) pore size distribution of the biomorphic ZnAl−MMO framework.

ing Information Figure S4 and Figure S5, respectively). Compared with the biotemplated LDH film, larger particles of ZnAl−LDH (20 nm in diameter) with higher crystallinity were observed for the powder sample (Figure S4), and the hexagonal lattice $a = 0.30$ nm was also determined. The powder sample of ZnAl−MMO also exhibits two different interplanar distances, that is, 0.46 nm corresponding to the (111) plane of cubic $ZnAl_2O_4$ and 0.26 nm for the (002) facet of hexagonal ZnO (Figure S5). The biomorphic MMO framework shows higher dispersion and lower crystallinity compared to the powder sample, possibly resulting from its ordered hierarchical structure.

Sorption Analysis. The biotemplated ZnAl−MMO framework was analyzed by nitrogen sorption measurement to shed light on its textural and pore size distribution properties. Figure 5A shows the nitrogen sorption isotherm of the ZnAl−MMO framework, and the pore size distribution was determined by means of the Barrett−Joyner−Halenda (BJH) model from the desorption branch of the nitrogen sorption isotherm (Figure 5B). The ZnAl−MMO framework (Figure 5A) exhibits a typical *IV* isotherm with a H3-type hysteresis loop ($P/P_0 > 0.4$), implying the presence of mesopores. Moreover, any limiting adsorption at higher P/P_0 cannot be observed, indicating the existence of macropores.[40] This result is further confirmed by the corresponding rather wide distribution of pore size in Figure 5B (3−30 nm, maximum at 3.76 nm). This is due to the hierarchical structure of the biomorphic ZnAl−MMO framework: mesopores result from an arrangement of nanocrystals of $ZnO/ZnAl_2O_4$ with the *ab* plane perpendicular to the substrate, while macropores originate from the tubal trichomas on the surface of the legume. However, a narrow pore diameter distribution (3−10 nm, maximum at 3.9 nm; see Supporting Information Figure S6) was observed for the powder sample, as a result of the accumulation of the nanocrystals. A high specific surface area (134.32 $m^2 \cdot g^{-1}$) for the biomorphic ZnAl−MMO framework was obtained owing to the monodispersion of nanocrystals, while the powder sample shows a specific surface area as low as 55.44 $m^2 \cdot g^{-1}$. In conclusion, the hierarchical structure and high dispersion of nanocrystals result in the wide pore size distribution and high specific surface area of the biomorphic ZnAl−MMO framework. This is preferable for the diffusion and transfer of reactants, which is a key factor influencing its catalytic performances.

Catalytic Performances. Hierarchically porous oxides have received considerable interest as a potential catalytic support or photocatalytic materials. The photocatalytic properties of the ZnAl−MMO framework catalyst for the decomposition of two dyes (PAZO and RB) were evaluated in this work. The ZnAl−MMO framework catalyst was immersed in the dye solution and irradiated with UV light from a mercury lamp. The absorption spectra of the solution as a function of irradiation time (at every 15 min interval over a period of 120 min) were recorded by using a UV−vis spectrometer. The self-degradations of both PAZO and RB were also studied by using the dye solution as a reference sample without any catalyst under the same irradiation conditions. The decomposed content of dye was calculated by C/C_0, where C and C_0 are the absorbance intensity of the sample at time intervals and initial, respectively. It was found that the molecule of PAZO does not degrade itself without any catalyst under irradiation of UV light (Figure 6A). However, the existence of the MMO catalyst favors the occurrence of this reaction. The catalytic degradation by the MMO powder sample was ~8.1% over 120 min, with the apparent first-order reaction rate constant of 0.0007 min^{-1}. In contrast, the fraction of the decomposed dye was ~29% by the biomorphic MMO framework with the apparent reaction constant of 0.0029 min^{-1}. In the case of RB (Figure 6B), obvious self-degradation was observed under irradiation of UV light, and the presence of MMO catalyst increases its degradation process significantly. The decomposition of RB by the biomorphic MMO framework reaches ~81% over 120 min (the apparent first-order

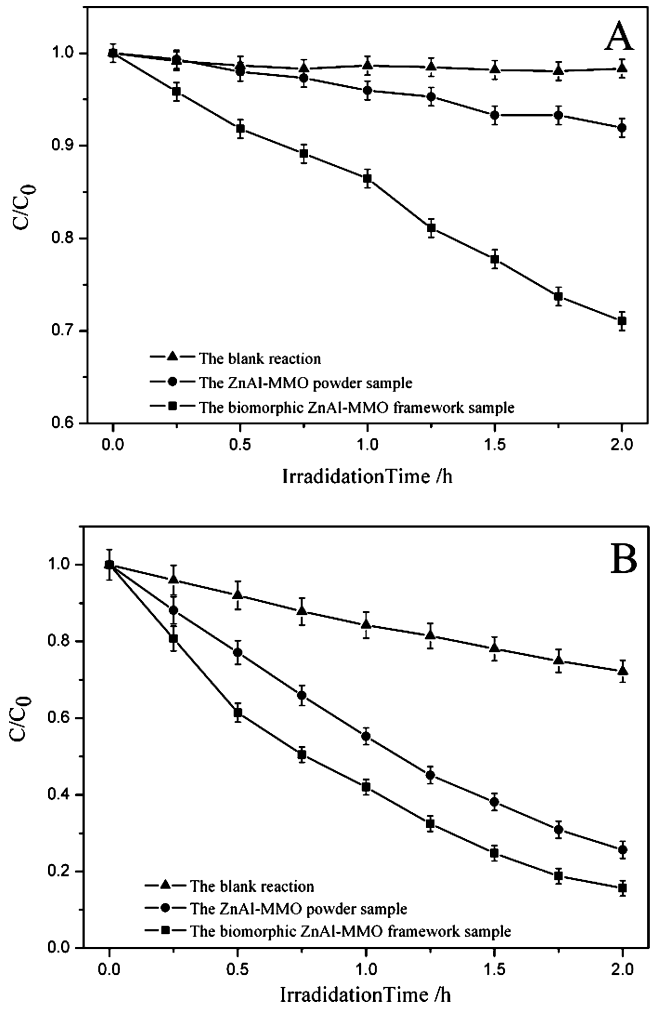

Figure 6. Photodegradation of (A) PAZO and (B) RB monitored as the normalized concentration *vs* irradiation time.

reaction rate constant 0.0159 min^{-1}), comparative to ~74% by the MMO powder sample (the apparent reaction rate constant 0.0120 min^{-1}). On the basis of the results above, it can be concluded that the biomorphic MMO framework exhibits much higher photocatalytic activity than that of the comparison powder sample, which is attributed to the hierarchical pores distribution as well as the higher BET surface area of the MMO framework. It was well-known that large surface area helps to increase the photocatalytic reaction sites and promote the efficiency of the electron−hole separation.[41] The macrochannels exhibit two beneficial effects on the photocatalyst, namely, increasing the efficiency of photoabsorption and improving mass transfer. In addition, the high dispersion of MMO nanocrystals and wide pore size distribution not only benefit the transfer of the light-generated charge carriers to the surface to react with dye molecules but also allow fast diffusion of reactants and products. However, it should be noted that the photocatalysis measurements in this work only give qualitative value for the reaction, and the intrapore mass transfer resistance as well as proportionality of reaction rate to internal surface area was unknown. The cyclic performance of the MMO framework was also tested, and the results demonstrate that it can serve as an effective and recyclable photocatalyst for even 6 times (Supporting Information Figure S7). Compared with the MMO powder sample, it can be concluded that the biotemplated MMO framework can be used as an excellent photocatalyst due to its large specific surface area and wide pore size distribution resulted from the hierarchical structure.

CONCLUSIONS

In summary, the present work demonstrates a general biotemplated methodology for the fabrication of hierarchically macro/mesoporous MMO framework. By using a combination of ALD−*in situ* growth−calcination, the biomorphic ZnAl−MMO framework was obtained with multilevel 3D morphologies from nanoscale to macroscale using legume as the sacrificial biotemplate. It was found that the MMO framework catalyst can be used as an effective and recyclable photocatalyst and exhibits higher photocatalytic activity than the corresponding MMO powder sample. This is due to the hierarchical structure of the biomorphic MMO framework along with a high specific surface area and wide pore size distribution (including mesopores and macropores). Therefore, it is anticipated that the new strategy reported in this work can be employed to fabricate various biotemplated LDH films as well as MMO frameworks. By virtue of the versatility of biotemplates and highly tunable compositions of inorganic LDH counterparts, these biomorphic materials can be potentially applied in the fields of catalysis and adsorption with enhanced efficiency. Our study demonstrates an exciting approach for enhancing the chemical performance of conventional catalysts through biomimicking.

METHODS

Deposition of Al_2O_3 onto the Surface of the Legume. Legumes were obtained from the campus of Beijing University of Chemical Technology and were washed thoroughly with pure water. The ALD deposition was performed in a Savannah 100 atomic layer deposition system. $Al(CH_3)_3$ (TMA) and deionized water ($R \approx 18$ MΩ) were used as precursors for alumina growth. The deposition was performed at 80 °C and under ~0.6 Torr chamber pressure. Ultrahigh purity N_2 was used as carrying and purging gas with a flow rate of 20 sccm. The Al_2O_3 film was fabricated layer-by-layer on the surface of the legume with precisely controlled wall thickness at a deposition rate of approximately 1 Å per cycle. Each deposition cycle (one monolayer) lasted 24 s, yielding a total deposition of 600 cycles (~60 nm).

Preparation of ZnAl−LDH/Legume Film. ZnAl−LDH/legume film was prepared by an *in situ* growth technique similar to a previous report by our group.[33] $Zn(NO_3)_2 \cdot 6H_2O$ (0.01 mol) and NH_4NO_3 (0.06 mol) were dissolved in deionized water (100 mL),

and the 1% ammoniaol solution was then slowly added until the pH reached 6.5. The Al_2O_3/legume substrate was placed in the above solution in an autoclave at 75 °C for 36 h. Finally, the substrate was removed, rinsed with ethanol, and dried at room temperature.

Preparation of ZnO−$ZnAl_2O_4$ Mixed Metal Oxide (MMO) Framework. The sample of the above synthesized Zn−Al LDH/legume precursor was calcined in air at 500 °C for 6 h, with a heating rate of 5 °C/min and held at every 100 °C for 0.5 h. The calcination process pyrolyzes the legume completely and converts the ZnAl−LDH into ZnAl−MMO at the same time. The resulting product was slowly cooled to room temperature.

Characterization. The powder XRD measurements were performed on a Rigaku XRD-6000 diffractometer, using Cu Kα radiation (λ = 0.15418 nm) at 40 kV, 30 mA, with a scan step of 0.02° and a 2θ angle ranging from 10 to 80°. The morphology of the film samples was investigated using a Hitachi S-3500N scanning electron microscope (SEM) with an accelerating voltage of 20 kV. Transmission electron microscopy (TEM) images were recorded with Philips TECNAI-20 and JEOL JEM-2010 high-resolution transmission electron microscopes. The accelerating voltage was 200 kV. Elemental analysis was performed using a Shimadzu ICPS-7500 inductively coupled plasma emission spectrometer (ICP-ES). Samples were dried at 100 °C for 24 h prior to analysis, and solutions were prepared by dissolving the samples in dilute hydrochloric acid (1:1). The specific surface area determination, pore volume, and size analysis were performed by BET and BJH methods using a Quantachrome Autosorb-1C-VP analyzer. Prior to the measurements, samples were degassed at 200 °C for 2 h.

Photocatalytic Reactions. The catalytic activities of the MMO framework were evaluated by the photocatalytic oxidation reaction of two dyes, that is, sulforhodamine B and poly{1-4[4-(3-carboxy-4-hydroxyphenylazo)benzenesulfonamido]-1,2-ethanediyl sodium salt} (PAZO). First, 3.5 mL of PAZO (1.0×10^{-5} M) or sulforhodamine B (1.0×10^{-5} M) solution was added to a typical quartz cell, and then 0.028 g of ZnAl−MMO framework catalyst was immersed into the solution. The powder sample of ZnAl−MMO was also prepared and evaluated as a comparison catalyst (see Supporting Information for preparation and characterization details). Then the quartz cells were placed side-by-side and irradiated with UV light produced from a mercury lamp. At given time intervals, the solution was analyzed by measuring the absorption band maximum using a Shimadzu UV-2501PC spectrophotometer. The procedure was performed for 6 cycles to evaluate the catalyst for multiple uses. The blank reaction was carried out following the same procedure without adding catalyst.

Acknowledgment. This work was supported by the National Natural Science Foundation of China, the 111 Project (Grant No. B07004), the 973 Program (Grant No. 2009CB939802), and the Program for Changjiang Scholars and Innovative Research Team in University (Grant No. IRT0406). The authors would like to thank Yongxi Shi for the assistance in HRTEM.

Supporting Information Available: Experimental procedures for the ZnAl−LDH powder and ZnAl−MMO powder sample; SEM image, XRD pattern, HRTEM image, and N_2 sorption isotherm and pore diameter distribution of the ZnAl−MMO powder sample; XRD pattern of the biomorphic ZnAl−MMO framework sample; photocatalytic behavior of the biotemplated ZnAl−MMO framework for the degradation of PAZO and RB over 6 cycles. This material is available free of charge *via* the Internet at http://pubs.acs.org.

REFERENCES AND NOTES

1. Yang, P. D; Deng, T.; Zhao, D. Y.; Feng, P. Y.; Pine, D.; Chmelka, B. F.; Whitesides, G. M.; Stucky, G. D. Hierarchically Ordered Oxides. *Science* **1998**, *282*, 2244–2266.
2. Kuang, D. B.; Brezesinski, T.; Smarsly, B. Hierarchical Porous Silica Materials with a Trimodal Pore System Using Surfactant Templates. *J. Am. Chem. Soc.* **2004**, *126*, 10534–10535.
3. Yuan, Z. Y.; Su, B. L. Insights into Hierarchically Meso/Macroporous Structured Materials. *J. Mater. Chem.* **2006**, *16*, 663–667.
4. Love, J. C.; Gates, B. D.; Wolfe, D. B.; Paul, K. E.; Whitesides, G. M. Fabrication and Wetting Properties of Metallic Half-Shells with Submicron Diameters. *Nano Lett.* **2002**, *2*, 891–894.
5. Li, D.; Xia, Y. Fabrication of Titania Nanofibers by Electrospinning. *Nano Lett.* **2003**, *3*, 555–560.
6. Chai, J.; Buriak, J. M. Using Cylindrical Domains of Block Copolymers To Self-Assemble and Align Metallic Nanowires. *ACS Nano* **2008**, *2*, 489–501.
7. Blin, J. L.; Leonard, A.; Yuan, Z. Y.; Gigot, L.; Vantomme, A.; Cheetham, A. K.; Su, B. L. Hierarchically Mesoporous/Macroporous Metal Oxides Templated from Polyethylene Oxide Surfactant Assemblies. *Angew. Chem., Int. Ed.* **2003**, *42*, 2872–2875.
8. Hang, Q.; Maschmann, M. R.; Fisher, T. S.; Janes, D. B. Assemblies of Carbon Nanotubes and Unencapsulated Sub-10-nm Gold Nanoparticles. *Small* **2007**, *3*, 1266–1271.
9. Dickey, M. D.; Weiss, E. A.; Smythe, E. J.; Chiechi, R. C.; Capasso, F.; Whitesides, G. M. Fabrication of Arrays of Metal and Metal Oxide Nanotubes by Shadow Evaporation. *ACS Nano* **2008**, *2*, 800–808.
10. Zampieri, A.; Schwieger, W.; Zollfrank, C.; Greil, P. Organic Preforms of Biological Origin: Natural Plant Tissues as Templates for Inorganic and Zeolitic Macrostructures. *Handbook of Biomineralization: Biomimetic and Bioinspired Chemistry*; Wiley-VCH Verlag GmbH & Co. KGaA: Weinheim, Germany, 2007; pp 255−288.
11. Sotiropoulou, S.; Sierra-Sastre, Y.; Mark, S. S.; Batt, C. A. Biotemplated Nanostructured Materials. *Chem. Mater.* **2008**, *20*, 821–834.
12. Mann, S. The Chemistry of Form. *Angew. Chem., Int. Ed.* **2000**, *39*, 3392–3406.
13. Mann, S. *Biomimetic Materials Chemistry*; VCH Publishers, Inc.: New York, 1996.
14. Davis, S. A.; Burkett, S. L.; Mendelson, N. H.; Mann, S. Bacterial Templating of Ordered Macrostructures in Silica and Silica−Surfactant Mesophases. *Nature* **1997**, *385*, 420–423.
15. Hall, S. R.; Bolger, H.; Mann, S. Morphosynthesis of Complex Inorganic Forms Using Pollen Grain Templates. *Chem. Commun.* **2003**, 2784–2785.
16. Bao, Z. H.; Weatherspoon, M. R.; Shian, S.; Cai, Y.; Graham, P. D.; Allan, S. M.; Ahmad, G.; Dickerson, M. B.; Church, B. C.; Kang, Z. T. Chemical Reduction of Three-Dimensional Silica Micro-assemblies into Microporous Silicon Replicas. *Nature* **2007**, *446*, 172–175.
17. Weatherspoon, M. R.; Cai, Y.; Crne, M.; Srinivasarao, M.; Sandhage, K. H. 3D Rutile Titania-Based Structures with Morpho Butterfly Wing Scale Morphologies. *Angew. Chem., Int. Ed.* **2008**, *47*, 7921–7924.
18. Huang, J. Y.; Wang, X. D.; Wang, Z. L. Controlled Replication of Butterfly Wings for Achieving Tunable Photonic Properties. *Nano Lett.* **2006**, *6*, 2325–2331.
19. Ogasawara, W.; Shenton, W.; Davis, S. A.; Mann, S. Template Mineralization of Ordered Macroporous Chitin-Silica Composites Using a Cuttlebone-Derived Organic Matrix. *Chem. Mater.* **2000**, *12*, 2835–2837.
20. Chia, S.; Urano, J.; Tamanoi, F.; Dunn, B.; Zink, J. I. Patterned Hexagonal Arrays of Living Cells in Sol−Gel Silica Films. *J. Am. Chem. Soc.* **2000**, *122*, 6488–6499.
21. Berry, V.; Rangaswamy, S.; Saraf, R. F. Highly Selective, Electrically Conductive Monolayer of Nanoparticles on Live Bacteria. *Nano Lett.* **2004**, *4*, 939–942.
22. Kim, S.-W.; Han, T. H.; Kim, J.; Gwon, H.; Moon, H.-S.; Kang, S.-W.; Kim, S. O.; Kang, K. Fabrication and Electrochemical Characterization of TiO_2 Three-Dimensional Nanonetwork Based on Peptide Assembly. *ACS Nano* **2009**, *3*, 1085–1090.
23. Samson, J.; Varotto, A.; Nahirney, P. C.; Toschi, A.; Piscopo, I.; Drain, C. M. Fabrication of Metal Nanoparticles Using Toroidal Plasmid DNA as a Sacrificial Mold. *ACS Nano* **2009**, *3*, 339–344.

24. Zampieri, A.; Mabande, G. T. P.; Selvam, T.; Schwieger, W.; Rudolph, A.; Hermann, R.; Sieber, H.; Greil, P. Biotemplating of Luffa Cylindrica Sponges to Self-Supporting Hierarchical Zeolite Macrostructures for Bio-inspired Structured Catalytic Reactors. *Mater. Sci. Eng., C* **2006**, *26*, 130–135.
25. Shin, H. C.; Corno, J. A.; Gole, J. L.; Liu, M. Porous Silicon Negative Electrodes for Rechargeable Lithium Batteries. *J. Power Sources* **2005**, *139*, 314–320.
26. Bengtsson, M.; Ekstrom, S.; Drott, J. Applications of Microstructured Porous Silicon as a Biocatalytic Surface. *Phys. Status Solidi A* **2000**, *182*, 495–504.
27. Li, F.; Duan, X. Applications of Layered Double Hydroxides. *Struct. Bonding* **2006**, *119*, 193–223.
28. Zou, L.; Li, F.; Xiang, X.; Evans, D. G.; Duan, X. Self-generated Template Pathway to High-Surface-Area Zinc Aluminate Spinel with Mesopore Network from a Single-Source Inorganic Precursor. *Chem. Mater.* **2006**, *18*, 5852–5859.
29. Gursky, J. A.; Blough, S. D.; Luna, C.; Gomez, C.; Luevano, A. N.; Gardner, E. A. Particle−Particle Interactions between Layered Double Hydroxide Nanoparticles. *J. Am. Chem. Soc.* **2006**, *128*, 8376–8377.
30. Gardner, E. A.; Huntoon, K. M.; Pinnavaia, T. J. Direct Synthesis of Alkoxide-Intercalated Derivatives of Hydrocalcite-like Layered Double Hydroxides: Precursors for the Formation of Colloidal Layered Double Hydroxide Suspensions and Transparent Thin Films. *Adv. Mater.* **2001**, *13*, 1263–1266.
31. Lee, J. H.; Rhee, S. W.; Jung, D. Y. Solvothermal Ion Exchange of Aliphatic Dicarboxylates into the Gallery Space of Layered Double Hydroxides Immobilized on Si Substrates. *Chem. Mater.* **2004**, *16*, 3774–3779.
32. Li, L.; Ma, R. Z.; Ebina, Y.; Fukuda, K.; Takada, K.; Sasaki, T. Layer-by-Layer Assembly and Spontaneous Flocculation of Oppositely Charged Oxide and Hydroxide Nanosheets into Inorganic Sandwich Layered Materials. *J. Am. Chem. Soc.* **2007**, *129*, 8000–8007.
33. Chen, H. Y.; Zhang, F. Z.; Fu, S. S.; Duan, X. *In Situ* Microstructure Control of Oriented Layer Double Hydroxide Monolayer Films with Curved Hexagonal Crystals as Superhydrophoboic Materials. *Adv. Mater.* **2006**, *18*, 3089–3093.
34. Zhang, F. Z.; Zhao, L. L.; Chen, H. Y.; Xu, S. L.; Evans, D. G.; Duan, X. Corrosion Resistance of Superhydrophobic Layer Double Hydroxide Film on Aluminum. *Angew. Chem., Int. Ed.* **2008**, *47*, 2466–2469.
35. Geraud, E.; Rafqah, S.; Sarakha, M.; Forano, C.; Prevot, V.; Leroux, F. Three Dimensionally Ordered Macroporous Layer Double Hydroxides: Preparation by Templated Impregnation/Coprecipitation and Pattern Stability upon Calcination. *Chem. Mater.* **2008**, *20*, 1116–1125.
36. Liu, C.; Wang, C.-C.; Kei, C.-C.; Hsueh, Y.-C.; Perng, T.-P. Atomic Layer Deposition of Platinum Nanoparticles on Carbon Nanotubes for Application in Proton-Exchange Membrane Fuel Cells. *Small* **2009**, *5*, 1535–1539.
37. Marotti, R. E.; Guerra, D. N.; Bello, C.; Machado, G.; Dalchiele, E. A. Bandgap Energy Tuning of Electrochemically Grown ZnO Thin Films by Thickness and Electrodeposition Potential. *Sol. Energy Mater. Sol. Cells* **2004**, *82*, 85–103.
38. Liu, J. P.; Li, Y. Y.; Huang, X. T.; Li, G. Y.; Li, Z. K. Layered Double Hydroxide Nano- and Microstructures Grown Directly on Metal Substrates and Their Calcined Products for Application as Li-Ion Battery Electrodes. *Adv. Funct. Mater.* **2008**, *18*, 1448–1458.
39. Jiang, P.; Zhou, J. J.; Fang, H. F.; Wang, C. Y.; Wang, Z. L.; Xie, S. S. Hierarchical Shelled ZnO Structures Made of Bunched Nanowire Arrays. *Adv. Funct. Mater.* **2007**, *17*, 1303–1310.
40. Zhou, L.; Wang, W. Z.; Xu, H. L.; Sun, S. M.; Shang, M. Bi_2O_3 Hierarchical Nanostructures: Controllable Synthesis, Growth Mechanism, and their Application in Photocatalysis. *Chem.—Eur. J.* **2009**, *15*, 1776–1782.
41. Wang, X. C.; Yu, J. C.; Ho, C. M.; Hou, Y. D.; Fu, X. Z. Photocatalytic Activity of a Hierarchically Macro/Mesoporous Titania. *Langmuir* **2005**, *21*, 2552–2559.